



## Accepted Author Manuscript

**Journal:** *Optics Letters*

**Article Title:** Raman amplification of optical beam carrying orbital angular momentum in a multimode step-index fiber

**Authors:** Shankar Pidishety, Sheng Zhu, Yutong Feng, Balaji Srinivasan, and Johan Nilsson

**Accepted for publication:** 26 February 2019

**Final version published:** 22 March 2019

**DOI:** <https://doi.org/10.1364/OL.44.001658>

# Raman amplification of optical beam carrying orbital angular momentum in a multimode step-index fiber

SHANKAR PIDISHETY,<sup>\*1</sup> SHENG ZHU,<sup>1</sup> YUTONG FENG,<sup>1</sup> BALAJI SRINIVASAN<sup>2</sup> AND JOHAN NILSSON<sup>1</sup>

<sup>1</sup>Optoelectronics Research Centre, University of Southampton, Southampton, SO171BJ, United Kingdom

<sup>2</sup>Department of Electrical Engineering, Indian Institute of Technology Madras, Chennai-600036, India

\*Corresponding author: [pd.shankara@gmail.com](mailto:pd.shankara@gmail.com)

Received XX Month XXXX; revised XX Month, XXXX; accepted XX Month XXXX; posted XX Month XXXX (Doc. ID XXXXX); published XX Month XXXX

**We experimentally demonstrate 15 dB of Raman amplification of 1115-nm pulses in an orbital angular momentum mode (OAMM) with charge  $l = +2$ ,  $S = +1$  in 5 m of step-index-25- $\mu\text{m}$ -diameter-core fiber. The total output reaches 4.5 kW of peak power and 68.5  $\mu\text{J}$  of energy in  $\sim 15$  ns pulses at 4 kHz repetition rate. An Yb-doped fiber source pumps the Raman amplifier at 1060 nm with 60-ns pulses. Using a spatial light modulator for modal decomposition, we measure 83% purity for the amplified target OAMM of selected polarization. To the best of our knowledge, this is the first time high energy, peak power, gain and purity are achieved in a fiber Raman amplifier for a single OAMM. © 2019 Optical Society of America**

**OCIS codes:** (080.4865) Optical vortices; (140.4480) Optical amplifiers; (230.2285) Fiber devices and optical amplifiers.

<http://dx.doi.org/10.1364/OL.99.099999>

Optical beams carrying orbital angular momentum (OAM) are attracting substantial research interest in a wide variety of fields ranging from high resolution imaging [1], nano-particle manipulation [2], positron and electron acceleration [3], and surface-plasmonic field excitation [4] to communication in classical [5,6] and quantum systems [7]. In many cases a power-scalable scheme capable of amplifying OAM beams with high mode-purity is required [3,6–8 and references therein]. Amplification of OAM beams has been investigated in a range of gain media, including rare-earth (RE) doped crystals [9] and optical fibers [10,11]. Generally, fiber amplifiers can provide high gain, high power, high efficiency and broad gain bandwidth [12], which are attractive features for spectrally and temporally versatile master oscillator-power amplifier (MOPA) sources [12]. Fiber MOPAs are increasingly used for power-scaling of beams with bespoke spatial properties [12,13], including OAM beams [10,11,14]. Since the

corresponding OAM modes (OAMMs) are higher order modes, they require multimode fibers. A key challenge is mode mixing. Also mode-selective gain saturation can degrade the mode, and is a special concern in case of saturated amplification of a single mode (e.g., an OAMM) [10,11]. Specially designed ring-core fibers can mitigate the degradation [15], but it is difficult to achieve the precise control of refractive index and active dopant distribution necessary to preserve the mode purity.

Fiber Raman amplifiers (FRAs) offer several additional attractions. Although largely unexplored, these are expected to apply also to OAMMs. Attractions include wavelength agility and low noise figure [16–18]. Furthermore, for multimode fibers, the non-local gain saturation and the relatively low mode-dependent gain (e.g., 0.25 dB for 10 dB gain [19]), are attractive for mode-agile amplification of a single mode as well as multiple simultaneous modes with high mode preservation. Fibers for Raman amplifiers normally use germano-silicate cores, just like conventional passive telecommunication fibers. The fabrication is very well established with control of longitudinal and transverse refractive index and circularity far superior to that of conventional fabrication processes for RE-doped fibers. Thus, passive fibers with ring-shaped cores designed for stable propagation of OAMMs can be readily used as Raman amplifiers by appropriate pumping, with unrivaled compatibility and with all-fiber signal excitation [15,20]. OAMM Raman amplification has been demonstrated recently in an 18-km-long fiber with moderate gain (3 dB) for telecommunication [21].

In this paper, we demonstrate Raman amplification of a single OAMM with  $l = +2$ ,  $S = +1$  ( $l$ -charge,  $S$ -circular polarization) in a MOPA configuration. A FRA based on a 5-m multimode step-index passive fiber amplifies  $\sim 15$ -ns-long pulses at 1115 nm by 15 dB of total average-power gain to 68.5  $\mu\text{J}$  energy, 4.5 kW peak power with 17.9% conversion efficiency. The mode purity is measured to be 83% in the amplified target OAMM of selected polarization. The present demonstration is significantly enhanced over the 6.5 dB gain value reported previously [17]. The

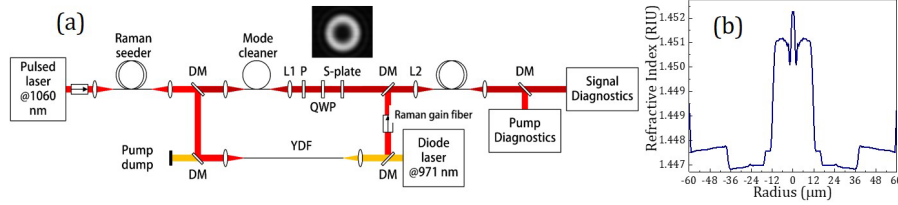


Fig. 1. (a) Schematic diagram of experimental setup with the inset showing the OAM beam profile after the S-plate. P: polarizer; QWP: quarter wave plate; S-plate (optical vortex converter), DM: dichroic mirror Diagnostics: ref. Fig (4). (b): Measured refractive index profile (RIP) of Raman gain fiber.

enhancement is attributed to improved pump coupling into the Raman gain fiber thanks to a lower-NA core in the Yb-doped fiber pump source [22], and improved characterization with real-time monitoring and quantification of the amplified OAMM purity.

Figure 1 shows a schematic of our experimental setup. This is the same as used in ref. [17] except for differences in the large-core YDF pump booster and the diagnostics [22]. Thus, a diode-seeded YDF-based source (G3, SPI Lasers) generates unpolarized 60-ns pulses at 4 kHz pulse repetition frequency (PRF) at 1060 nm with  $\sim 8$  nm linewidth. The pulses are launched into a 30-m-long Ge-doped silica fiber (Freelight, Pirelli) to generate signal radiation at 1115 nm via stimulated Raman scattering (SRS). The 1115-nm signal and residual 1060-nm pump pulses are separated by a dichroic mirror (DM) at the fiber output. Subsequently, in one arm of the setup, the 1115-nm pulses are mode-cleaned in a 3-m-long perpendicularly cleaved passive single-mode fiber (1060-XP, Nufern). This also length-matches the signal and pump beam paths. The resulting Gaussian-like mode is then collimated by an aspheric lens ( $f = 8$  mm), after which a polarizer, a quarter-waveplate (QWP), and an S-wave plate with 72% transmission converts it to the desired circularly polarized OAM beam of  $l = +2$  [17,23]. The resulting OAM beam is then precisely launched into 5 m of multimode step-index Raman gain fiber (25/125  $\mu\text{m}$ , NA 0.12, OFS Inc. call no. 35275) by an aspheric lens ( $f = 15$  mm) with 41% launch efficiency. The gain fiber comprises a 30-cm-diameter coil and both ends are cleaved perpendicularly. Fig. 1 (b) shows its refractive index profile.

In the other arm of the setup, the 1060-nm pump energy that remains after the Freelight fiber is boosted to 1.3 mJ in 5 m of in-house-fabricated YDF (55/725  $\mu\text{m}$  diameter, NA 0.09, absorption 3.8 dB/m at the 976-nm peak) with a  $\sim 4^\circ$  angle-cleaved output end. This is pumped by a 971 nm CW diode laser (LDL 80-500, Laserline). The amplified 1060-nm pulses are recombined with the 1115-nm OAM signal pulses by a DM and are then launched through an aspheric lens ( $f = 15$  mm) into the Raman gain fiber with  $\sim 30\%$  launch efficiency. The Raman gain is only present during the pump pulses, so these are temporally overlapped with the OAM signal pulses through the path length-matching. At the output of the Raman gain fiber, the amplified OAM signal and residual pump beams are collimated by an aspheric lens ( $f = 11$  mm), and separated by another DM. A thermal power meter, 350 MHz Si detectors (DET10A2, Thorlabs) connected to a 6 GHz oscilloscope (Infiniium 54855A, Agilent), and an optical spectrum analyzer (OSA) (AQ6317B, Ando) are used for average-power, temporal, and spectral measurements. The mode purity of the amplified OAMM is measured with a mode decomposition apparatus comprising a reflective spatial light modulator (SLM-

100, Santec) and a CMOS camera (DCC1545M, Thorlabs).

First, we describe the gain and pump depletion measurement results, shown in Fig. 2 (a) as a function of launched pump peak power. The corresponding optical spectra are shown in Fig. 2 (b). The Raman gain, which is calculated as the ratio between the time-averaged total signal output power with and without pumping, grows almost linearly with pump power. The pump depletion is calculated as  $(P_2 - P_1)/P_2$ , where  $P_1$  and  $P_2$  are the transmitted average pump power with and without Raman seeding, respectively. Since the unseeded average Stokes output power is only  $\sim 7$  mW at maximum pump power, we ignore pump depletion from unseeded SRS. At maximum gain, for 382  $\mu\text{J}$  of energy and 6.95 kW of peak and 1.53 W of average pump power (launched), we reach 68.5  $\mu\text{J}$  total signal pulse energy and 4.5 kW peak power with 20% pump depletion and 17.9% pump-to-signal conversion efficiency. The gain slope of 2.15 dB/kW corresponds to a Raman gain coefficient of 48.7 fm/W, which agrees well with the expected value for un-polarized pumping at 1060 nm [24]. The gain grows nearly linearly with pump power, despite the 20% depletion. The depletion occurs primarily near the output end and therefore reduces the Raman gain in only a short length of fiber.

Figure 3 shows measured temporal traces of the output signal pulse without pumping and with 15 dB gain, as well as the corresponding launched pump pulse. The oscilloscope traces were visually un-broadened, indicating good short-term stability. Long-term, the pump and signal peak values drifted by  $\sim 5\%$ , primarily attributed to drifts in power coupled into the Freelight fiber. We observe a minor peak  $\sim 50$  ns after the main peak in the amplified signal trace. Since this time equals the roundtrip propagation time in the Raman gain fiber, we attribute the peak to amplification of signal light doubly Fresnel-reflected from the perpendicularly cleaved fiber ends. Such multi-pass amplification is a particular concern when the pump pulse is comparable to, or longer than, the

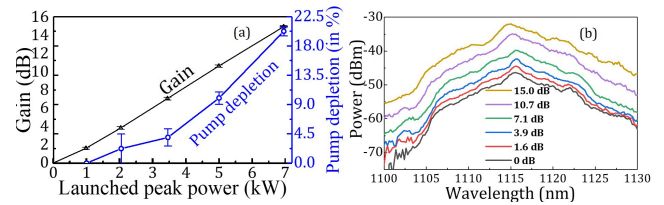


Fig. 2. (a): Measured gain for the total average power in all modes and pump depletion vs. launched pump peak power (with error bars). (b): Optical spectra (measured by the OSA in average-power mode with 0.2 nm resolution) for average-power gains as indicated.

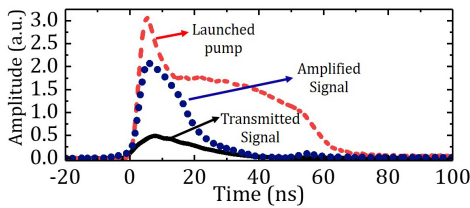


Fig. 3. Output signal pulses without pumping (solid black curve) and at 15 dB gain (dotted blue curve) and launched pump pulses (dashed red curve). Curves are plotted with different amplitude scaling.

round-trip propagation time. We estimate the total backward signal output power to 10-20% of the forward power.

The mode purity of the amplified OAM signal is a key metric. We measured this by decomposing the output signal beam into an OAM basis set with a spatial light modulator (SLM) based setup [25] shown in Fig. 4. A QWP converts the OAMM's output polarization from circular to linear. This is then oriented to the SLM's working polarization plane (horizontal) by a half-waveplate (HWP) and a polarizer. The overall polarization purity was determined as the fraction of power transmitted by the polarizer at 0 dB gain. This was 94%. This high degree of preservation of circular polarization suggests that the linear birefringence is low in our fiber [15,26]. Furthermore, the use of an unpolarized pump means that the Raman amplification is polarization-independent. Thus, we disregard the polarization effects in the fiber and the power rejected by the polarizer in our mode purity assessment.

A series of computer-generated forked holograms possessing different OAM charge from  $l = -4$  to  $+4$  and with fringe pitch of  $\sim 136 \mu\text{m}$  are formed on the SLM. Primarily, the holograms serve to change the azimuthal phase between the incident and diffracted beam. The far-field profile of the first-order beam as diffracted from the SLM and collected by a telescope comprising a  $fL3 = 100 \text{ mm}$  transform lens and a  $fL4 = 75 \text{ mm}$  imaging lens is recorded by a CMOS camera (Fig. 4). An aperture rejects other diffraction orders. The on-axis intensity of the recorded far-field diffraction pattern is proportional to the square of the integral of the complex amplitude of the field leaving the SLM [26]. This becomes zero when fiber modes with uncompensated charge are integrated azimuthally. The contributions to the on-axis intensity of OAMMs with compensated charge are proportional to the modal power, but with different constants of proportionality because of differences in the radial dependence of the modes. OAMMs with  $l \neq 0$  are characterized by donut-shaped distributions with one or several rings. The sign of the amplitude alternates between rings, which leads to cancellation in the diffracted on-axis intensity for higher radial mode orders (i.e., with several rings). However, for OAMMs of the lowest radial order and with  $l \neq 0$ , there is only one ring. For those, the differences in the radial distribution of modes with different charge can be assumed to be relatively small, and the constant of proportionality between the on-axis intensity and the power in such modes approximately the same, as the SLM pattern sweeps from  $l = -4$  to  $+4$ . Furthermore, we estimated the constant of proportionality of the fundamental mode to be  $\sim 80\%$  of that of our target mode. Higher charges are not

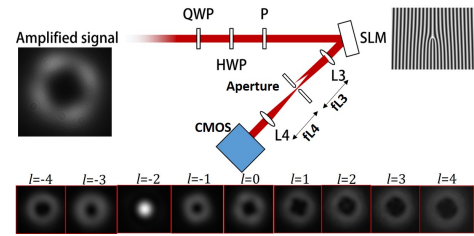


Fig. 4. Experimental setup for mode purity measurement. Images of the transmitted signal (left) and the far-field (bottom) of the first order diffraction from the SLM for different  $l$  (image brightness increased for better visibility), and a sample forked SLM pattern of  $l = -2$  (right).

supported by the gain fiber. The first higher radial order is supported for  $l = 0, \pm 1$ , but the power in those modes is expected to be small (see below). Therefore, we neglected the impact of power in those modes and determined the relative power in the different charges and thus the mode purity of the targeted OAMM under the assumption that the power in a charge is dominated by the power in a single OAMM, with the same proportionality to the on-axis intensity. Note also that the 8-nm linewidth means that except for conjugate pairs, uncoupled modes are expected to be mutually incoherent.

Initially, without pumping, the purity of the incident and transmitted OAMM is measured to  $\sim 97.4\%$  and  $\sim 95.8\%$  in the selected polarization, respectively. This suggests that the purity degrades by only  $\sim 1.5\%$ . We conclude that the fiber is well capable of preserving the target OAMM (including its polarization). The relative content of the output beam for different charges is shown in Fig. 5, for 0 dB as well as 15 dB of average-power gain. However, the purity degrades approximately linearly with gain, from 95.8% at 0 dB to 83.2% at 15 dB. See the inset in Fig. 5.

There are several possible reasons for the purity degradation, including mode-selective gain saturation, mode-coupling in the fiber, and degraded launch alignment. Fig. 5 shows that coupling into the conjugate  $l = -2$  OAMM alone accounts for around 50% of the overall degradation in purity. This has the same modal intensity distribution as the targeted  $l = +2$  mode, so relative to this, it would not be any less affected by, and thus not explained by, mode-selective gain saturation resulting from mode-selective pump depletion. Furthermore, a misaligned launch is not expected to couple light into  $l = -2$  with significant selectivity. Regarding mode-coupling, we calculated all effective indices  $n_{\text{eff}}$  of the OAMMs, including their spin-orbit aligned and anti-aligned states, from the measured refractive index profile in Fig. 1 (b) using COMSOL Multiphysics® eigenmode solver. Depending on spin,  $l = +2$  and  $l = -2$  OAMMs are degenerate or quasi-degenerate with splitting  $\Delta n_{\text{eff}}$  of  $\sim 10^{-7}$ . Given the minimum index separation of  $\sim 10^{-4}$  RIU generally used as a criterion for stable propagation of OAMMs over long distances [15], fiber imperfections and bends may well couple power into  $l = -2$  [15,18,27]. Indeed, our experiments show small ( $< 1\%$ ) improvements in mode purity when the coil diameter of the gain fiber is increased from an initial value of  $\sim 30 \text{ cm}$ . Thus, we believe that coupling between quasi-degenerate modes during propagation is the primary cause of purity degradation, although further work is needed to clarify and if possible reduce the dependence on the gain level. By contrast, coupling to other modes

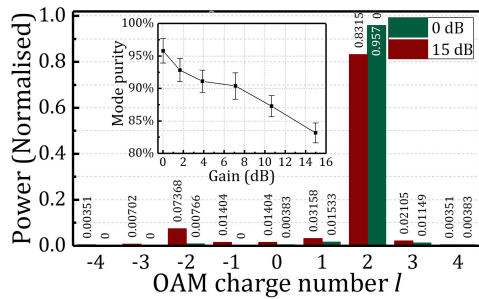


Fig. 5. Experimentally measured fraction of power in modes vs. charge for 0 dB and 15 dB gain. Inset: Mode purity of the  $l = +2$  OAMM as a function of total average power gain (with errors bars).

during propagation is expected to be small, since the differences in effective index from the modes of  $l = \pm 2$  to  $l = \pm 1$  and  $l = \pm 3$  are  $\sim 3.5 \times 10^{-4}$  RIU. Fig. 4 confirms this. We note that  $l = 0$  and  $l = \pm 1$  support higher-order radial modes which conceivably could carry power which is not represented well by the on-axis intensity. However,  $\Delta n_{\text{eff}}$  is even larger to those modes ( $\sim 1.4 \times 10^{-3}$ ), which are therefore expected to carry less power than the nearest OAMMs of  $l = \pm 1$  and  $l = \pm 3$ . Thus, we believe the mode purity error this introduces is negligible. As it comes to mode-selective gain saturation, this would favour the fundamental mode, because of its low intensity overlap with our target mode. However, the on-axis intensity for  $l = 0$  is low in Fig. 4. This indicates that mode-selective gain saturation does not significantly degrade the mode purity.

We also note that it was possible to increase the pump power further and thus increase the gain to about 18 dB and depletion to about 30%. However, then unseeded SRS became relatively high and the mode purity degraded substantially. For gain beyond 15 dB, the backward output power may exceed the forward power, depending on the pump pulse duration, shape, and depletion. If this is mode-selective then it can also lead to rapidly increasing unseeded SRS in unwanted modes. In future work, fiber end-capping may alleviate such problems and allow for higher gain by reducing the feedback from end-facets. Although outside our primary scope, also the temporal stability and noise properties may improve by end-capping at high gain. This together with a pulse shape closer to rectangular may also improve the efficiency.

In conclusion, we have experimentally demonstrated Raman amplification of OAMM of  $l = +2$  in a 5 m step-index passive fiber with up to 15 dB total average-power gain with multimode pumping. The mode purity is well-preserved throughout the amplification, dropping from 95.8% at 0-dB gain to 83.2% at 15-dB gain, in the selected polarization. The amplified OAMM of  $l = +2$  degrades mainly by coupling power into its conjugate OAMM of  $l = -2$ . Possible mode degradation mechanisms such as mode-selective gain saturation, mode-coupling in the fiber, and degraded launch alignment are discussed based on the observed experimental results. Similar behavior was observed for amplification of an OAMM of the same absolute charge ( $l = -2$ ), but generally, OAMM stability is charge dependent and needs to be investigated for other charges. Given that the conversion efficiency reached 17.9% and that the fiber supports  $\sim 40$  pump modes, we estimate that the brightness improved by 8 dB from launched pump to signal. We believe that our spectrally flexible and brightness-enhancing amplification approach through stimulated Raman scattering is an attractive option for amplifying beams possessing OAM.

All data supporting this study are available from the University of Southampton at <https://doi.org/10.5258/SOTON/D0745>.

**Funding.** AFOSR (FA2386-16-1-0005, FA2386-16-1-4077).

**Acknowledgment.** We thank Yongmin Jung, Peter Kazansky and Pranabesh Barua, University of Southampton, Christophe Codemard, SPI Lasers, and Vijay Kumar, IISER Pune, Srinivas P, IIT Madras, for fruitful discussions and loan of components.

## References

1. L. Yan, P. Gregg, E. Karimi, A. Rubano, L. Marrucci, R. Boyd, and S. Ramachandran, *Optica* **2**, 900 (2015).
2. M. Padgett and R. Bowman, *Nat. Photonics* **5**, 343 (2011).
3. J. Vieira and J. T. Mendonça, *Phys. Rev. Lett.*, **112**, 215001 (2014).
4. S. Pidishety, V. Kumar, N. K. Viswanathan, *Opt. Lett.* **37**, 4233 (2012).
5. A. E. Willner, H. Huang, Y. Yan, Y. Ren, N. Ahmed, G. Xie, C. Bao, L. Li, Y. Cao, Z. Zhao, J. Wang, M. P. J. Lavery, M. Tur, S. Ramachandran, A. F. Molisch, N. Ashrafi, and S. Ashrafi, *Adv. Opt. Photon.*, **7**, 66 (2015).
6. Y. Ren, L. Li, Z. Wang, S. M. Kamali, E. Arbabi, A. Arbabi, Z. Zhao, G. Xie, Y. Cao, N. Ahmed, Y. Yan, C. Liu, A. J. Willner, S. Ashrafi, M. Tur, A. Faraon, and A. E. Willner, *Scientific Reports* **6**, 33306 (2016).
7. M. Erhard, R. Fickler, M. Krenn, and A. Zeilinger, *Light: Science & Applications* **7**, 17146 (2018).
8. J. Vieira, R. M. G. M. Trines, E. P. Alves, R. A. Fonseca, J. T. Mendonça, R. Bingham, P. Norreys, and L. O. Silva, *Nat. Commun.*, **7**, 10371 (2016).
9. X. Chen, C. Chang, Z. Lin, P. Ding, and J. Pu, *IEEE Photonics Technol. Lett.*, **28**, 1271 (2016).
10. Q. Kang, P. Gregg, Y. Jung, E. L. Lim, S. Alam, S. Ramachandran, and D. J. Richardson, *Opt. Express* **23**, 28341 (2015).
11. Y. Jung, Q. Kang, R. Sidharthan, D. Ho, S. Yoo, P. Gregg, S. Ramachandran, S.-U. Alam, and D. J. Richardson, *J. Lightwave Technol.*, **35**, 430 (2017).
12. D. J. Richardson, J. Nilsson, and W. A. Clarkson, *J. Opt. Soc. Am. B* **27**, B63 (2010).
13. D. Lin, N. Baktash, S. Alam, D. J. Richardson, *Opt. Lett.*, **43**, 4957 (2018).
14. M. Koyama, T. Hirose, M. Okida, K. Miyamoto, and T. Omatu, *Opt. Express* **19**, 14420 (2011).
15. P. Gregg, P. Kristensen, and S. Ramachandran, *Optica* **2**, 267 (2015).
16. V. R. Supradeepa, Y. Feng, J. W. Nicholson, *J. Opt.* **19**, 023001 (2017).
17. S. Pidishety, S. Zhu, P. G. Kazansky, J. Nilsson, and B. Srinivasan, in *Laser Congress 2017 (ASSL, LAC) (2017)*, p. JTh2A.6 (Optical Society of America, 2017).
18. S. Zhu, S. Pidishety, Y. Feng, S. Hong, J. Demas, R. Sidharthan, S. Yoo, S. Ramachandran, B. Srinivasan, J. Nilsson, *Opt. Express*, **26**, 23295 (2018).
19. E. N. Christensen, J. G. Koefoed, S. M. M. Friis, M. A. U. Castaneda, and K. Rottwitz, *Scientific Reports* **6**, 34693 (2016).
20. S. Pidishety, S. Pachava, P. Gregg, S. Ramachandran, G. Brambilla, and B. Srinivasan, *Opt. Lett.*, **42**, 4347 (2017).
21. L. Zhu, J. Li, G. Zhu, L. Wang, C. Cai, A. Wang, S. Li, M. Tang, Z. He, S. Yu, C. Du, W. Luo, J. Liu, J. Du, and J. Wang, in *Optical Fiber Communication Conference*, p. W4C.4 (Optical Society of America, 2018).
22. S. Zhu, S. Pidishety, and J. Nilsson, in *Laser Congress 2018 (ASSL) (2018)*, p. AW2A.4 (Optical Society of America, 2018).
23. M. Beresna, M. Gecevičius, P. G. Kazansky, and T. Gertus, *Appl. Phys. Lett.* **98**, 201101 (2011).
24. G. Agrawal, *Nonlinear Fiber Optics* (Academic Press, 2013).
25. B. M. Heffernan, R. D. Niederriter, M. E. Siemens, and J. T. Gopinath, *Opt. Lett.*, **42**, 2683 (2017).
26. J. W. Goodman, *Introduction to Fourier Optics* (Roberts and Company Publishers, 2005).
27. Z. Ma, G. Prabhakar, P. Gregg, S. Ramachandran, *Conf. on Lasers and Electro-Optics (2018)*, p. SW3K.1 (Optical Society of America, 2018).

## References in full:

1. L. Yan, P. Gregg, E. Karimi, A. Rubano, L. Marrucci, R. Boyd, and S. Ramachandran, "Q-plate enabled spectrally diverse orbital-angular-momentum conversion for stimulated emission depletion microscopy," *Optica* **2**(10), 900 (2015).
2. M. Padgett and R. Bowman, "Tweezers with a twist," *Nature Photonics* **5**(6), 343–348 (2011).
3. J. Vieira and J. T. Mendonça, "Nonlinear Laser Driven Donut Wakefields for Positron and Electron Acceleration," *Phys. Rev. Lett.* **112**(21), 215001 (2014).
4. S. Pidishety, V. Kumar, and N. K. Viswanathan, "Plasmon-mediated vectorial topological dipole: formation and annihilation," *Optics letters* **37**(20), 4233–4235 (2012).
5. A. E. Willner, H. Huang, Y. Yan, Y. Ren, N. Ahmed, G. Xie, C. Bao, L. Li, Y. Cao, Z. Zhao, J. Wang, M. P. J. Lavery, M. Tur, S. Ramachandran, A. F. Molisch, N. Ashrafi, and S. Ashrafi, "Optical communications using orbital angular momentum beams," *Adv. Opt. Photon.*, **7**(1), 66–106 (2015).
6. Y. Ren, L. Li, Z. Wang, S. M. Kamali, E. Arbabi, A. Arbabi, Z. Zhao, G. Xie, Y. Cao, N. Ahmed, Y. Yan, C. Liu, A. J. Willner, S. Ashrafi, M. Tur, A. Faraon, and A. E. Willner, "Orbital Angular Momentum-based Space Division Multiplexing for High-capacity Underwater Optical Communications," *Scientific Reports* **6**, 33306 (2016).
7. M. Erhard, R. Fickler, M. Krenn, and A. Zeilinger, "Twisted photons: new quantum perspectives in high dimensions," *Light: Science & Applications* **7**(3), 17146 (2018).
8. J. Vieira, R. M. G. M. Trines, E. P. Alves, R. A. Fonseca, J. T. Mendonça, R. Bingham, P. Norreys, and L. O. Silva, "Amplification and generation of ultra-intense twisted laser pulses via stimulated Raman scattering," *Nature Communications* **7**, 10371 (2016).
9. X. Chen, C. Chang, Z. Lin, P. Ding, and J. Pu, "High-Energy Nanosecond Optical Vortex Output From Nd:YAG Amplifiers," *IEEE Photonics Technology Letters* **28**(12), 1271–1274 (2016).
10. Q. Kang, P. Gregg, Y. Jung, E. L. Lim, S. Alam, S. Ramachandran, and D. J. Richardson, "Amplification of 12 OAM Modes in an air-core erbium doped fiber," *Optics Express* **23**(22), 28341 (2015).
11. Y. Jung, Q. Kang, R. Sidharthan, D. Ho, S. Yoo, P. Gregg, S. Ramachandran, S.-U. Alam, and D. J. Richardson, "Optical Orbital Angular Momentum Amplifier Based on an Air-Hole Erbium-Doped Fiber," *J. Lightwave Technol.*, **35**(3), 430–436 (2017).
12. D. J. Richardson, J. Nilsson, and W. A. Clarkson, "High power fiber lasers: current status and future perspectives [Invited]," *J. Opt. Soc. Am. B, JOSAB* **27**(11), B63–B92 (2010).
13. D. Lin, N. Baktash, S. Alam, and D. J. Richardson, "106W, picosecond Yb-doped fiber MOPA system with a radially polarized output beam," *Opt. Lett.*, **43**(20), 4957–4960 (2018).
14. M. Koyama, T. Hirose, M. Okida, K. Miyamoto, and T. Omatsu, "Nanosecond vortex laser pulses with millijoule pulse energies from a Yb-doped double-clad fiber power amplifier," *Opt. Express*, **19**(15), 14420–14425 (2011).
15. P. Gregg, P. Kristensen, and S. Ramachandran, "Conservation of orbital angular momentum in air-core optical fibers," *Optica* **2**(3), 267 (2015).
16. V. R. Supradeepa, Y. Feng, and J. W. Nicholson, "Raman fiber lasers," *J. Opt.* **19**(2), 023001 (2017).
17. S. Pidishety, S. Zhu, P. G. Kazansky, J. Nilsson, and B. Srinivasan, "Amplification of Orbital Angular Momentum Beam in a Fiber Raman Amplifier," in *Laser Congress 2017 (ASSL, LAC) (2017), Paper JTh2A.6* (Optical Society of America, 2017).
18. S. Zhu, S. Pidishety, Y. Feng, S. Hong, J. Demas, R. Sidharthan, S. Yoo, S. Ramachandran, B. Srinivasan, and J. Nilsson, "Multimode-pumped Raman amplification of a higher order mode in a large mode area fiber," *Opt. Express*, **26**(18), 23295–23304 (2018).
19. E. N. Christensen, J. G. Koefoed, S. M. M. Friis, M. A. U. Castaneda, and K. Rottwitt, "Experimental characterization of Raman overlaps between mode-groups," *Scientific Reports* **6**, 34693 (2016).
20. S. Pidishety, S. Pachava, P. Gregg, S. Ramachandran, G. Brambilla, and B. Srinivasan, "Orbital angular momentum beam excitation using an all-fiber weakly fused mode selective coupler," *Opt. Lett.*, **42**(21), 4347–4350 (2017).
21. L. Zhu, J. Li, G. Zhu, L. Wang, C. Cai, A. Wang, S. Li, M. Tang, Z. He, S. Yu, C. Du, W. Luo, J. Liu, J. Du, and J. Wang, "First Demonstration of Orbital Angular Momentum (OAM) Distributed Raman Amplifier over 18-km OAM Fiber with Data-Carrying OAM Multiplexing and Wavelength-Division Multiplexing," in *Optical Fiber Communication Conference*, p. W4C.4 (OSA, 2018).
22. S. Zhu, S. Pidishety, and J. Nilsson, "15-dB Raman Amplification of an Optical Orbital Angular Momentum Mode in a Step-Index Fiber," in *Laser Congress 2018 (ASSL) (2018), p.AW2A.4* (Optical Society of America, 2018).
23. M. Beresna, M. Gecevičius, P. G. Kazansky, and T. Gertus, "Radially polarized optical vortex converter created by femtosecond laser nanostructuring of glass," *Appl. Phys. Lett.* **98**(20), 201101 (2011).
24. G. Agrawal, *Nonlinear Fiber Optics* (Academic Press, 2013).
25. B. M. Heffernan, R. D. Niederriter, M. E. Siemens, and J. T. Gopinath, "Tunable higher-order orbital angular momentum using polarization-maintaining fiber," *Opt. Lett.*, **42**(14), 2683–2686 (2017).
26. J. W. Goodman, *Introduction to Fourier Optics* (Roberts and Company Publishers, 2005).
27. Z. Ma, G. Prabhakar, P. Gregg, and S. Ramachandran, "Robustness of OAM fiber modes to geometric perturbations," in *Conference on Lasers and Electro-Optics (2018), p. SW3K.1* (Optical Society of America, 2018).